

Processing telecom wavelength light with an optically tunable memory

David P. Lake,¹ Matthew Mitchell,¹ and Paul. E. Barclay¹

Department of Physics and Astronomy and Institute for Quantum Science and Technology, University of Calgary, Calgary, AB, T2N 1N4, Canada^{a)}

(Dated: 13 December 2019)

Information storage and processing devices are essential elements of classical and quantum communication and computing technologies. Optical memories based on optomechanically induced transparency allow storage of optical signals in the motion of mechanical resonators. However, their storage time is limited by intrinsic mechanical dissipation, and deterministic in-situ control and manipulation of the stored signals—i.e. processing—has not been demonstrated. Here, we address both of these limitations using reservoir engineering of the environment coupled to the mechanical resonator. We demonstrate that in-situ optomechanical control of the resonator’s mechanical properties can extend the optomechanical memory storage time, as well as deterministically shift the phase of a stored pulse by over 2π , expanding the information processing toolkit provided by cavity optomechanics.

Real-world optical, electrical, and mechanical devices exhibit dissipation due to their coupling to external degrees of freedom. This permits energy to leave and fluctuations to enter the system¹, and typically degrades the performance of information processing components such as memories. Reservoir engineering uses dissipation to enhance a system’s properties². For example, this technique allows preparation of trapped ions with external coupling to carefully tailored reservoirs into desirable quantum states³. Here we show that when reservoir engineering is extended to incorporate dynamic control of external coupling, a system’s steady state can be adiabatically manipulated. By applying such dynamic reservoir engineering to an optomechanical memory, we demonstrate that stored information can be coherently modified. This is a crucial step towards realizing full temporal control of quantum states of light stored in an optomechanical system.

I. RESULTS

In this article, we use coherent multimode optomechanics to transfer and store information input to the optical mode (a) of a diamond microdisk cavity in the device’s mechanical mode (b), while simultaneously modifying the mechanical mode’s dynamics through its coupling to a second ‘reservoir’ optical mode (r), as illustrated in Fig. 1. Microdisks can operate as multimode cavity optomechanical systems whose optical whispering gallery modes are coupled by radiation pressure to motion of the device’s mechanical radial breathing mode resonance⁴. Coherent multimode optomechanical coupling is possible in diamond microdisks even at room temperature and ambient conditions thanks to their low optical and mechanical loss combined with their ability to support intense intracavity fields without suffering from nonlinear absorption. Multimode cavity optomechanical devices

enable wavelength conversion^{5–8}, entanglement between photons^{9,10}, and low-noise frequency conversion¹¹. As we will show here, they are also excellent platforms for implementing reservoir engineering^{12,13}. In this work, the reservoir is driven by a control laser whose detuning, Δ_r , sets the phase lag of its optomechanical coupling to the resonator, and whose power, P_r , sets the coupling strength. This tunable resonator–reservoir interaction induces mechanical dissipation Γ_r^{opt} and shifts the mechanical resonator frequency by ω_r^{opt} , two effects widely studied in single-mode optomechanical systems, for example in demonstration of mechanical ground state cooling^{14,15}. In our multimode system, we dynamically tune the reservoir coupling to process information stored in the mechanical memory, whose dynamics we show are governed by:

$$\dot{\hat{b}} = - \left(i\omega_b^{\text{eff}}(t) + \frac{\Gamma_b^{\text{eff}}(t)}{2} \right) \hat{b} + \sqrt{\Gamma_b} \hat{e}_{\text{in}} + g_r \sqrt{\kappa_r} \chi_r(\omega_b; \Delta_r) \hat{r}_{\text{in}} + g_r \sqrt{\kappa_r} \chi_r^\dagger(\omega_b; \Delta_r) \hat{r}_{\text{in}}^\dagger, \quad (1)$$

where \hat{b} is the phonon annihilation operator, \hat{e}_{in} is the thermal bath input field, \hat{r}_{in} is the optical reservoir input field, and g_r is the photon assisted optomechanical coupling rate (see Supplementary Material). The key feature that we test and exploit is the ability to dynamically control the memory’s effective mechanical frequency, $\omega_b^{\text{eff}} = \omega_b + \omega_r^{\text{opt}}(t)$, and effective damping, $\Gamma_b^{\text{eff}} = \Gamma_b + \Gamma_r^{\text{opt}}(t)$ via the reservoir. We find that the memory operates *as if* it is a conventional optomechanical system composed of the renormalized mechanical resonator interacting with the ‘signal’ mode a . In this regime, which is valid if the mechanical dissipation rate $\Gamma_b \ll \kappa_r$ where κ_r is the reservoir’s optical decay rate (here $\Gamma_b/2\pi \sim 200$ kHz, $\kappa_r/2\pi \sim 1$ GHz), the control laser becomes an input to b filtered by the reservoir mode’s optical response χ_r in the frame of the control laser (see Supplementary Material).

Below we test the validity of this description and demonstrate applications of dynamic reservoir coupling through three experiments. First, we demonstrate a means to enhance the system’s optomechanical coopera-

^{a)}Electronic mail: pbarclay@ucalgary.ca

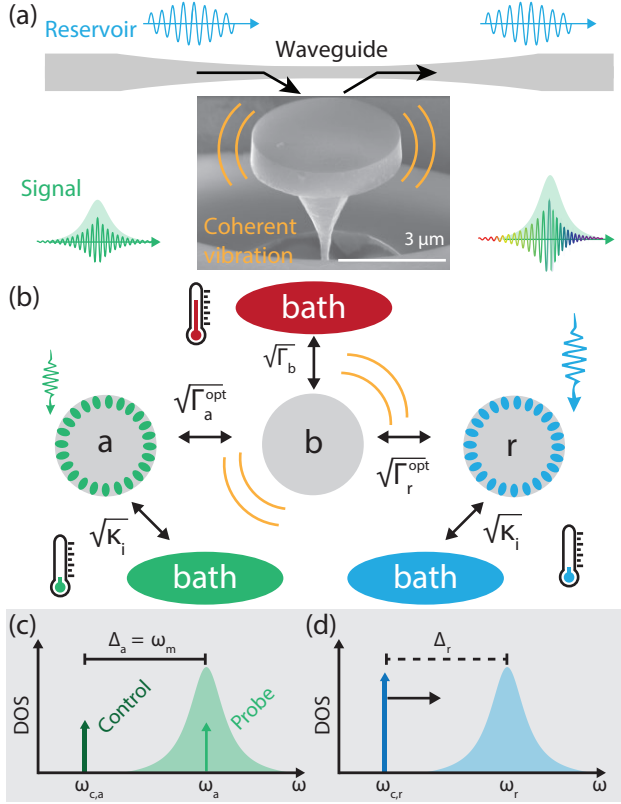


FIG. 1: (a) Annotated scanning electron micrograph of the diamond microdisk optomechanical cavity. A tapered optical fiber is utilized to couple two colors of light to the microdisk which in turn is coupled to mechanical vibrations of the radial breathing mode of the microdisk. (b) Schematic of the system under study where the mechanical mode b is coupled to the environment (red bath), a reservoir, r , and optical mode a , at the indicated rates. While coupling of the mechanical mode to the surrounding environment is an intrinsic property of the device and environment, the coupling to r may be manipulated through the use of a control laser. (c) Density of states picture showing the detuning of the control and probe laser fields for mode a (green) and mode r (blue).

tivity, and switch the dynamics of the system from overall loss to overall gain. Second, we demonstrate an enhancement in the optomechanical memory's storage time through control of Γ_b^{eff} . Finally, we demonstrate that the phase of a stored mechanical pulse may be controlled through manipulation of ω_b^{opt} .

A. Reservoir engineering

As a first test of reservoir engineering, we probe how the dynamics of the mechanical resonator, and its resulting coupling to light, are affected by the resonator-reservoir interaction. This is accomplished using optomechanically induced transparency (OMIT) spectroscopy^{16,17}. OMIT creates a transparency window in the cavity lineshape whose properties depend on the dynamics of the optomechanical system. By coher-

ently coupling a probe field in a to the mechanical resonator for varying reservoir control laser settings, we can learn about the influence of the reservoir on the resonator. These measurements are shown in Fig. 2(a), which were obtained using a fiber taper waveguide to evanescently couple the reservoir control laser to mode r ($\omega_r/2\pi = 192$ THz, $\kappa_r/2\pi = 1.13$ GHz) for varying Δ_r , while performing OMIT spectroscopy on mode a ($\omega_a/2\pi = 197$ THz, $\kappa_a/2\pi = 0.856$ GHz) using a weak resonant probe laser and a control laser red detuned by ω_b (see Methods). The device used here has $\omega_b/2\pi \sim 2.14$ GHz and operates in the resolved sideband regime for modes a and r ($\omega_b/\kappa_a = 2.5$, $\omega_b/\kappa_r = 1.9$). This measurement was repeated for three different values of P_r . At each reservoir setting Γ_b^{eff} and ω_b^{eff} were extracted from the OMIT window shape (see Supplementary Material), and are plotted along with fits to the data in Figs. 2(b) and (c). The fits, which show excellent agreement with measurements, were obtained with g_r as the only fitting parameter. This confirms that optical spring effects from the reservoir field manifest in changes to resonator dynamics experienced by the spectrally isolated field in mode a . Note that the optical reservoir mode is a standing wave doublet (see Methods) formed from backscattering in the microdisk^{18,19}, whose most apparent effect is the two sets of minima and maxima in Fig. 2(a), as well as related features in Figs. 2(b) and (c). In all measurements the mode a control field detuning was set relative to the lowest frequency doublet feature.

The system dynamics in the above measurements are most dramatically affected when Γ_b^{eff} approaches zero. In a conventional OMIT system, the depth and width of the transparency window is parameterized by the optomechanical cooperativity, $C = \frac{4|g_a|^2}{\kappa_a\Gamma_b}$, where g_a and κ_a are the photon-assisted optomechanical coupling and optical cavity energy decay rates for a , respectively. However, in our multimode system OMIT is governed by an effective cooperativity $C_{\text{eff}} = C \times \Gamma_b/\Gamma_b^{\text{eff}}$. In the measurement presented here we achieve a maximum $C_{\text{eff}} = 83$, which represents an enhancement of $158\times$ the bare $C \sim 0.5$, in absence of the reservoir field. This allows our system to act as though it has large cooperativity, enabling large light delays and narrow transparency windows (see Supplementary Material). In principle this enhancement is limited only by drift in Δ_r , which dictates how close to zero Γ_b^{eff} can be, and is not limited by the optomechanical coupling rate.

As Γ_b^{eff} becomes negative, the mechanical resonator motion changes from experiencing an overall loss to an overall gain. Consequently, by adjusting our reservoir coupling, we are able to tune the system dynamics between OMIT and the regime of optomechanically induced amplification (OMIA). This gain would normally cause optomechanically induced self-oscillation to occur^{20,21}. However, this instability is repressed in our multimode measurements by the optomechanical damping Γ_a^{opt} induced by the a mode OMIT process, provided

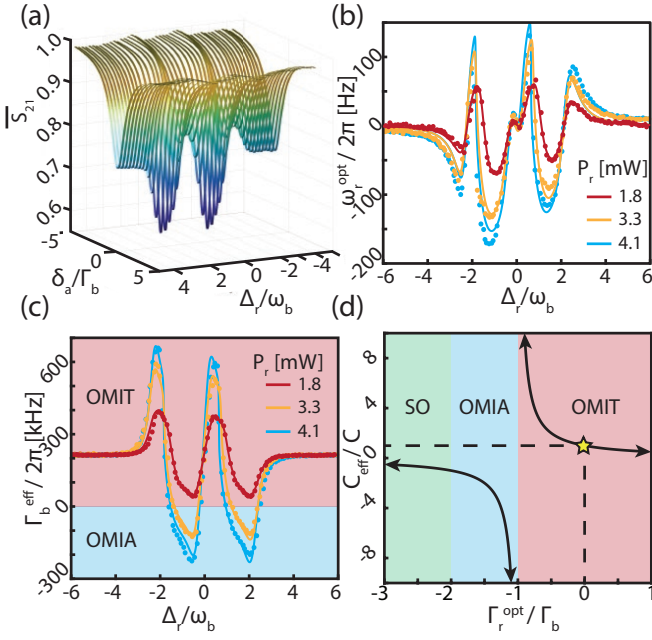


FIG. 2: (a) Normalized OMIT scans as a function of mode a probe-cavity detuning, δ_a , and control-reservoir detuning, Δ_r , measured via the fiber taper transmission. The changes in the transparency window as a function of Δ_r are indicative of reservoir interactions. Optomechanically manipulated effective (b) mechanical frequency and (c) damping as a function of Δ_r and the reservoir mode input power, P_r . (d) Illustration of effective cooperativity, C_{eff} , for varying Γ_b^{eff} controlled by the reservoir mode, when $\Gamma_b^{\text{eff}} = \Gamma_b$ due to the presence of the mode a fields. Three different regimes of operation are shown: OMIT, OMIA, and self-oscillation (SO).

$\Gamma_a^{\text{opt}} + \Gamma_b^{\text{eff}} > 0$. The ability of the reservoir mode to tune the system dynamics between OMIT, OMIA and self-oscillation regimes is illustrated in Fig. 2(f) for the special case that $\Gamma_a^{\text{opt}} = \Gamma_b$. In our measurements the OMIA regime was entered for the $P_r = 3.3$ mW and $P_r = 4.1$ mW settings when the control laser was blue detuned from the reservoir mode's lowest frequency doublet feature by approximately ω_b .

B. Pulse storage manipulation

Pioneering experiments in quantum optics utilizing Λ -type atomic systems have demonstrated that a strong control field can dramatically alter the optical properties of a material, including rendering otherwise opaque materials transparent²², enhancing nonlinear processes^{23,24}, and slowing the group velocity of a pulse of light^{25,26}. Furthermore, by dynamically altering the transparency of a material, a pulse of light may be trapped and deterministically released at a later time^{27–30}. Such schemes have been used to store light pulses for over a minute³¹, and have been proven to be a viable means to store single photons^{32,33}.

Inspired by these experiments with atoms, cavity op-

to mechanical systems have been shown to support analogous processes. In the OMIT^{16,17} spectroscopy measurements introduced above, the interaction between optical mode a and the mechanical resonator is governed by the beamsplitter Hamiltonian $\hat{H}_{\text{bs}} = \hbar g_a (\hat{a}^\dagger \hat{b} + \hat{a} \hat{b}^\dagger)$ when mode a 's control field is red detuned by ω_b from resonance³⁴. Here \hat{a} (\hat{a}^\dagger) and \hat{b} (\hat{b}^\dagger) are annihilation (creation) operators for optical mode a and mechanical resonator mode b , respectively. By adjusting the control field amplitude, which in turn controls g_a , a field input to a can be coherently and reversibly stored in the mechanical resonator.

Here we show that reservoir engineering can be harnessed to dynamically modify the information stored in an optomechanical memory. Our memory protocol is illustrated using mass-on-spring systems in Fig. 3(a). During the write stage, the red-detuned mode a control laser couples a weak signal field resonant with mode \hat{a} to mode \hat{b} at rate g_a . Following the write stage the control laser is removed and modes a and b are decoupled. Our scheme then deviates from a conventional optomechanical memory^{35–37} in two ways: not only is coupling to the reservoir turned on, which modifies the mechanical resonator dynamics as described above, the reservoir coupling is also varied temporally. This step both modifies the stored information and the rate at which it dissipates. Finally, during the read stage, the reservoir control laser is removed and the signal control laser is turned back on, reconverting the stored mechanical signal to the optical domain.

Through continuous amplification of the stored mechanical pulse by the reservoir mode, the pulse storage lifetime of the mechanical resonator can be extended by nearly an order of magnitude. This is in a similar spirit to previous demonstrations of optomechanical amplification in waveguides³⁸. To measure the storage time for a given reservoir setting, we varied the delay τ_d between the write and read pulses. The measured amplitude output during the read pulse encodes the temporal envelope of the mechanical signal, which decays exponentially at a rate Γ_b^{eff} . An example of this decay is plotted in Fig. 3(b) for two cases: when the reservoir control is optimally detuned for enhanced storage time ($\Delta_r \approx -\omega_b$ and $\Gamma_b^{\text{eff}} \ll \Gamma_b$), and when the reservoir is far detuned ($\Delta_r \gg \omega_b$ and $\Gamma_b^{\text{eff}} \sim \Gamma_b$). Comparing the observed decay rates for each configuration indicates a $7\times$ enhancement in storage time from $1.1 \mu\text{s}$ to $7.7 \mu\text{s}$ due to the reservoir coupling. Examples of the signal extracted at two values of τ_d are shown on Fig. 3(c,d), demonstrating the dramatic difference in the amplitude of the enhanced versus the unenhanced signal at longer timescales.

A full measurement of the readout amplitude decay for varying Δ_r was also acquired, the results of which are plotted in Fig. 3(e). This shows qualitative agreement to the theoretical amplitudes obtained from an analytic fit of $\Gamma_b^{\text{eff}}(\Delta_r)$ and plotted in Fig. 3(f). Note that the broad Δ_r range used in this measurement reveals the doublet

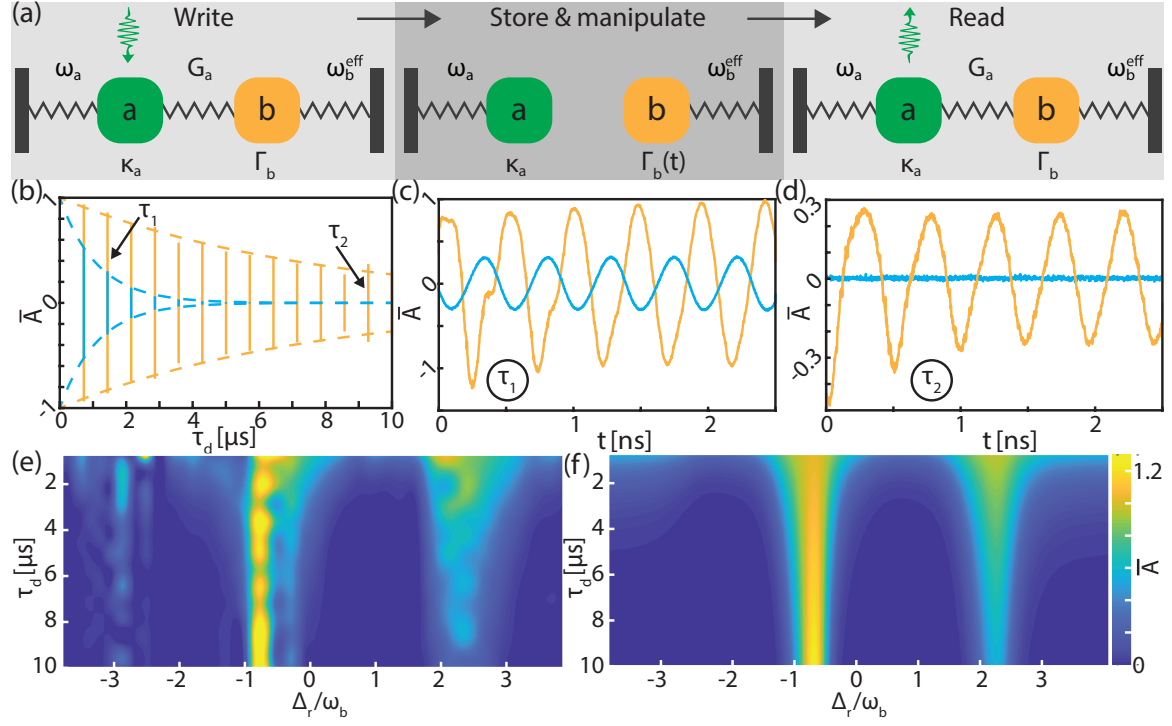


FIG. 3: (a) Outline of pulse storage protocol where the optomechanical coupling between optical mode a and the mechanical mode facilitates storage of an optical pulse as a mechanical excitation. Mode r is used to manipulate the mechanical damping rate, $\Gamma_b^{\text{eff}}(t)$, and frequency, $\omega_b^{\text{eff}}(t)$ which can be carried out concurrently with the storage process. (b) Normalized read pulse amplitude, \bar{A} for the off-resonant, $\Delta_r \gg \omega_m$, case (cyan) and for $\Delta_r \sim \omega_m$ (orange) as a function of τ_d . These are fit to an exponential decay (dashed lines) to extract Γ_b^{eff} . (c,d) Zoom-in of the read data shown in (b) for $\tau_d = (0.14, 0.93) \mu\text{s}$, illustrating the enhancement in \bar{A} when $\Delta_r \sim \omega_m$. (e) Complete data set from which (b) was taken showing both an enhancement and reduction in storage time as a function of Δ_r , which is compared to the expected behavior (f).

nature of the reservoir mode. Deviations between theory and experiment are understood to be a consequence of long-term thermal drifts in the resonance frequencies of the modes, as well as wavelength drifts in the readout laser used in the experiment. Note that this amplification process cannot be used indefinitely as the thermal phonons present due to the room temperature bath will eventually overwhelm the stored signal phonons, as described in the Supplementary Material.

Finally, we demonstrate that the phase of the stored pulse can be controlled via the reservoir mode. By changing ω_b^{eff} adiabatically and hence the frequency of the stored pulse, we can complete a trajectory which moves away from and then returns to the original frequency. Over the course of this trajectory, the mechanical oscillator acquires a dynamical phase $\varphi(t_2) = \varphi(t_1) + \int_{t_1}^{t_2} \delta\omega(t)dt$, assuming that we return to the original mechanical frequency. This is analogous to a pendulum whose length is adjusted in time³⁹. In our experiment, we varied the amplitude of the reservoir mode in time using an amplitude electro-optic modulator driven by a symmetric RF ramp pulse (see Supplementary Material) for various Δ_r as shown in Fig. 4(a). Here the ramp pulse was $3.5 \mu\text{s}$ long and was situated $1.5 \mu\text{s}$ after the write, and before the read pulse. By fitting the beat

note detected at the fiber output for each of the write, ramp, and read pulse segments we can plot the phase as referenced to the well-defined write pulse, as shown in shown in Fig. 4(b). Here we have removed the phase shift associated with the spring effect induced by the write pulse, which added a linear slope to the ramp and read pulse segments. This allows us to isolate the shift due to the spring effect associated with the reservoir mode ramp pulse (see Supplementary Material). From the read pulse segments we extract the phase relative to the write pulse, demonstrating a reservoir controlled phase shift, $\Delta\varphi > 2\pi$ as shown in Fig. 4(c).

II. DISCUSSION

In this work we have demonstrated that the in-situ control offered by reservoir engineering is a powerful tool for enhancement of storage times, bypassing the usual limitations imposed by the intrinsic damping rate, and can be used to generate controllable phase shifts in the stored pulse. For optomechanical devices in the sideband resolved regime ($\omega_b > \kappa$), Γ_b^{eff} and ω_b^{eff} are linearly independent in g_r and Δ_r ⁴⁰. Extending our work to incorporate dynamic control the damping rate would enable pulse compression by the realization of a time lens⁴¹.

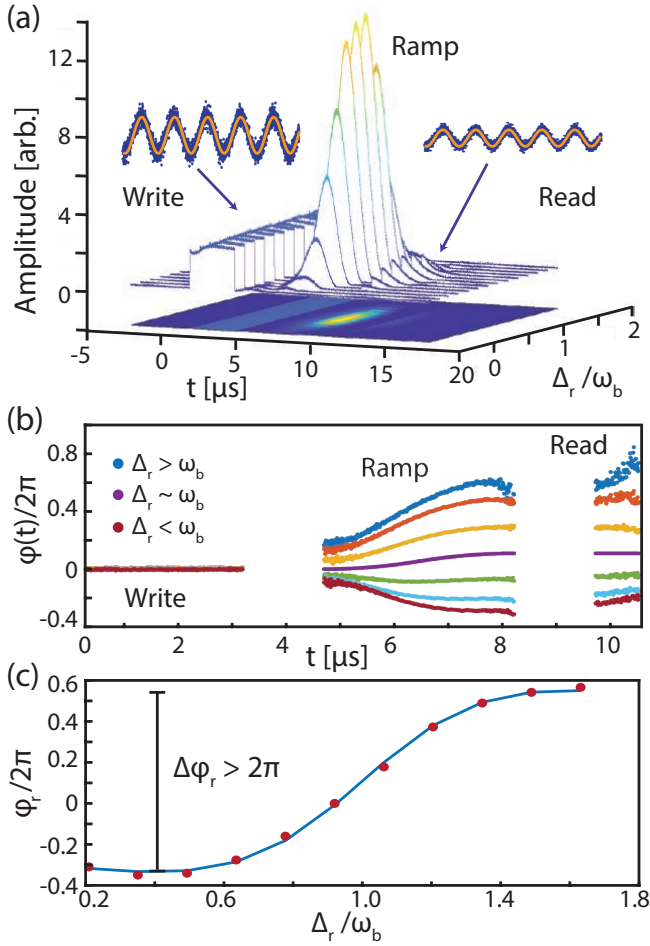


FIG. 4: (a) Amplitude of the acquired signals vs. time and reservoir detuning for the phase manipulation experiment. In this experiment no optical filtering was used, so that the write, ramp, and read pulses may all be detected. (b) Phase of the mechanical oscillator vs. time as inferred from the optical output of the device. (c) Final phase as a function of Δ_r along with a fit to the data based on the predicted temporally varying optical spring effect associated with the ramp pulse.

Furthermore, multiple pulses could be used in succession to realize very large phase shifts and pulse compression. As a localized mechanical mode is being used here, long storage times are possible^{35–37}, however, there is an associated inherent bandwidth limitation on the length of pulses that can be effectively stored, in contrast to Brillouin scattering devices^{38,42,43}. The long storage times enabled by this protocol will enable longer interaction times for interfacing the stored mechanical pulse with other systems, such as spins, or mechanical or electric fields. The demonstrated phase manipulation techniques also highlights this systems potential for use as a logic gate, where the stored pulse is interfered with an incoming optical pulse. Operating in the quantum regime is possible by cryogenically cooling the device to mK temperatures, which would enable shaping of stored single photons⁴⁴.

- ¹H. B. Callen and T. A. Welton, Phys. Rev. **83**, 34 (1951).
- ²J. F. Poyatos, J. I. Cirac, and P. Zoller, Phys. Rev. Lett. **77**, 4728 (1996).
- ³D. Kienzler, H.-Y. Lo, B. Keitch, L. de Clercq, F. Leupold, F. Lindenfesler, M. Marinelli, V. Negnevitsky, and J. P. Home, Science **347**, 53 (2015).
- ⁴M. Mitchell, B. Khanaliloo, D. P. Lake, T. Masuda, J. P. Hadden, and P. E. Barclay, Optica **3**, 963 (2016).
- ⁵J. T. Hill, A. H. Safavi-Naeini, J. Chan, and O. Painter, Nat. Commun. **3**, 1196 (2012).
- ⁶C. Dong, V. Fiore, M. C. Kuzyk, and H. Wang, Science **338**, 1609 (2012).
- ⁷Y. Liu, M. Davanço, V. Aksyuk, and K. Srinivasan, Phys. Rev. Lett. **110**, 223603 (2013).
- ⁸M. Mitchell, D. P. Lake, and P. E. Barclay, Optica **6**, 832 (2019).
- ⁹S. Barzanjeh, E. S. Redchenko, M. Peruzzo, M. Wulf, D. Lewis, and J. M. Fink, Nature **570**, 480 (2019).
- ¹⁰J. Chen, M. Rossi, D. Mason, and A. Schliesser, arXiv:1911.05729 (2019).
- ¹¹C. Ockeloen-Korppi, E. Damskägg, J.-M. Pirkkalainen, T. Heikkilä, F. Massel, and M. Sillanpää, Phys. Rev. X **6**, 041024 (2016).
- ¹²L. D. Tóth, N. R. Bernier, A. Nunnenkamp, A. K. Feofanov, and T. J. Kippenberg, Nat. Phys. **13**, 787 (2017).
- ¹³K. Fang, J. Luo, A. Metelmann, M. H. Matheny, F. Marquardt, A. A. Clerk, and O. Painter, Nat. Phys. **13**, 465 (2017).
- ¹⁴J. Chan, T. P. M. Alegre, A. H. Safavi-Naeini, J. T. Hill, A. Krause, S. Groblacher, M. Aspelmeyer, and O. Painter, Nature **478**, 89 (2011).
- ¹⁵J. Teufel, T. Donner, D. Li, J. Harlow, M. Allman, K. Cicak, A. Sirois, J. D. Whittaker, K. Lehnert, and R. W. Simmonds, Nature **475**, 359 (2011).
- ¹⁶S. Wei, R. Rivière, S. Deléglise, E. Gavartin, O. Arcizet, A. Schliesser, and T. J. Kippenberg, Science **330**, 1520 (2010).
- ¹⁷A. H. Safavi-Naeini, T. M. Alegre, J. Chan, M. Eichenfield, M. Winger, Q. Lin, J. T. Hill, D. Chang, and O. Painter, Nature **472**, 69 (2011).
- ¹⁸T. J. Kippenberg, S. M. Spillane, and K. J. Vahala, Opt. Lett. **27**, 1669 (2002).
- ¹⁹M. Borselli, T. J. Johnson, and O. Painter, Opt. Express **13**, 1515 (2005).
- ²⁰H. Rokhsari, T. J. Kippenberg, T. Carmon, and K. J. Vahala, Opt. Express **13**, 5293 (2005).
- ²¹M. Poot, K. Fong, M. Bagheri, W. Pernice, and H. Tang, Phys. Rev. A **86**, 053826 (2012).
- ²²K.-J. Boller, A. Imamoglu, and S. E. Harris, Phys. Rev. Lett. **66**, 2593 (1991).
- ²³M. Jain, A. Merriam, A. Kasapi, G. Yin, and S. Harris, Phys. Rev. Lett. **75**, 4385 (1995).
- ²⁴K. Hakuta, M. Suzuki, M. Katsuragawa, and J. Z. Li, Phys. Rev. Lett. **79**, 209 (1997).
- ²⁵A. Kasapi, M. Jain, G. Yin, and S. E. Harris, Physical review letters **74**, 2447 (1995).
- ²⁶L. V. Hau, S. E. Harris, Z. Dutton, and C. H. Behroozi, Nature **397**, 594 (1999).
- ²⁷C. Liu, A. Dutton, C. H. Behroozi, and L. V. Hau, Nature **409**, 490 (2001).
- ²⁸D. F. Phillips, A. Fleischhauer, A. Mair, R. L. Walsworth, and M. D. Lukin, Phys. Rev. Lett. **86**, 783 (2001).
- ²⁹M. R. Sprague, P. S. Michelberger, T. F. M. Champion, D. G. England, J. Nunn, X.-M. Jin, W. S. Kolthammer, A. Abdolvand, P. S. J. Russell, and I. A. Walmsley, Nat. Photonics **8**, 287 (2014).
- ³⁰D. G. England, K. A. G. Fisher, J.-P. W. MacLean, P. J. Bustard, R. Lausten, K. J. Resch, and B. J. Sussman, Phys. Rev. Lett. **114**, 053602 (2015).
- ³¹G. Heinze, C. Hubrich, and T. Halfmann, Phys. Rev. Lett. **111**, 033601 (2013).
- ³²T. Chaneliere, D. Matsukevich, S. Jenkins, S.-Y. Lan, T. Kennedy, and A. Kuzmich, Nature **438**, 833 (2005).

- ³³M. D. Eisaman, A. Andre, F. Massou, M. Fleischhauer, A. S. Zibrov, and M. D. Lukin, *Nature* **438**, 837 (2005).
- ³⁴M. Aspelmeyer, T. J. Kippenberg, and F. Marquardt, *Rev. Mod. Phys.* **86**, 1391 (2014).
- ³⁵V. Fiore, C. Dong, M. C. Kuzyk, and H. Wang, *Phys. Rev. A* **87**, 023812 (2013).
- ³⁶T. Palomaki, J. Harlow, J. Teufel, R. Simmonds, and K. Lehnert, *Nature* **495**, 210 (2013).
- ³⁷A. Wallucks, I. Marinković, B. Hensen, R. Stockill, and S. Gröblacher, *arXiv:1910.07409* (2019).
- ³⁸B. Stiller, M. Merklein, C. Wolff, K. Vu, P. Ma, S. J. Madden, and B. J. Eggleton, *arXiv:1904.13167* (2019).
- ³⁹H. Goldstein, *Classical Mechanics* (Addison Wesley, San Francisco, 2002).
- ⁴⁰H. Xu, D. Mason, L. Jiang, and J. G. E. Harris, *Nature* **537**, 80 (2016).
- ⁴¹G. Patera, J. Shi, D. B. Horoshko, and M. I. Kolobov, *J. Opt.* **19**, 054001 (2017).
- ⁴²D. J. G. Zhaoming Zhu and R. W. Boyd, *Science* **318**, 1748 (2007).
- ⁴³M. Merklein, B. Stiller, K. Vu, S. J. Madden, and B. J. Eggleton, *Nat. Commun.* **8**, 574 (2017).
- ⁴⁴O. Morin, M. Körber, S. Langenfeld, and G. Rempe, *Phys. Rev. Lett.* **123**, 133602 (2019).
- ⁴⁵M. Mitchell, D. P. Lake, and P. E. Barclay, *APL Photonics* **4**, 016101 (2019).

METHODS

A. Fabrication

The microdisks studied here were fabricated from an optical grade, chemical vapor deposition (CVD) grown (100)-oriented SCD substrate supplied by Element Six, according to the process outlined in detail in Ref.⁴⁵. The polished substrates were first cleaned in boiling piranha, and coated with ~ 400 nm of PECVD Si_3N_4 as a hard mask. To avoid charging effects during electron beam lithography (EBL), ~ 5 nm of Ti was deposited before the ZEP 520A EBL resist. The developed pattern was transferred to the hard mask via inductively coupled reactive ion etching (ICPRIE) with $\text{C}_4\text{F}_8/\text{SF}_6$ chemistry. The anisotropic ICPRIE diamond etch was performed using O_2 , followed by deposition of ~ 250 nm of conformal PECVD Si_3N_4 as a sidewall protection layer. The bottom of the etch windows were then cleared of Si_3N_4 using a short ICPRIE etch with $\text{C}_4\text{F}_8/\text{SF}_6$. This was followed by a zero RF power O_2 RIE diamond undercut etch to partially release the devices. The undercutting process was interrupted and an ~ 100 nm layer of SiO_2 is deposited via electron beam evaporation to alter the microdisk pedestal profile before finishing the undercut. Lastly, the Si_3N_4 layer was removed using a wet-etch in 49% HF, and the devices were cleaned again in boiling piranha.

B. Apparatus

The measurement apparatus for the results described in the main text is shown in Fig. 5, where the opti-

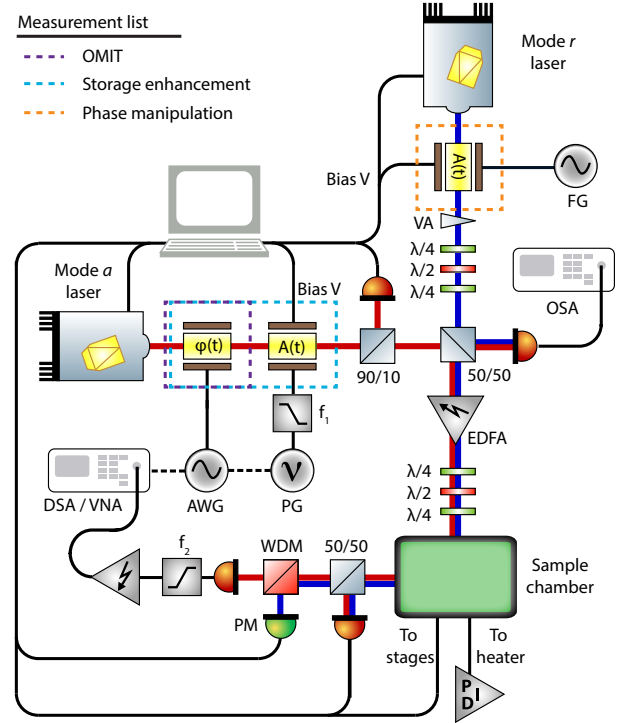


FIG. 5: Measurement setup including the components necessary for all measurements described in the main text. Legend indicates the optical components necessary for each measurement presented and the components are discussed in detail in the text.

cal components added for each measurement described in the main text are outlined in the legend. Mode a was driven by a tunable diode laser at 1560 nm (Newport TLB-6700) while the reservoir mode, r , was also driven by a tunable diode laser at 1520 nm (Newport TLB-6700) whose output was connected to a variable attenuator (VA: Exfo FVA-3100). For the verification of mutual coherence the mode a laser was passed through a phase electro-optic modulator ($\varphi(t)$: EOSpace PM-5S5-20-PFA-PFA-UV-UL) to generate a weak probe field from the control field, which was swept across the resonance using a vector network analyzer (VNA: Keysight E5063A) allowing the measurement of OMIT. The mode r laser was combined with the mode a laser on a fiber coupled 50/50 beamsplitter (BS: Newport F-CPL-L22355-A) where one output was sent to an erbium doped fiber amplifier (EDFA: Pritel LNHPFA-30-IO) and the other to an optical spectrum analyzer (OSA: Ando AQ6317B) such that the laser wavelengths could be tracked during the experiment. The output of the EDFA was sent to a fiber polarization unit followed by the fiber taper waveguide coupled to the diamond microdisk. The output of the fiber taper was then split on another 50/50 beamsplitter where one output is sent to a power meter (PM: Newport 1936-R) and one to a 1510/1550 nm wavelength division multiplexer (WDM: Montclair MFT-MC-51-30 AFC/AFC-1) to separate the light from modes a and r . The output of the WDM was then measured on a high

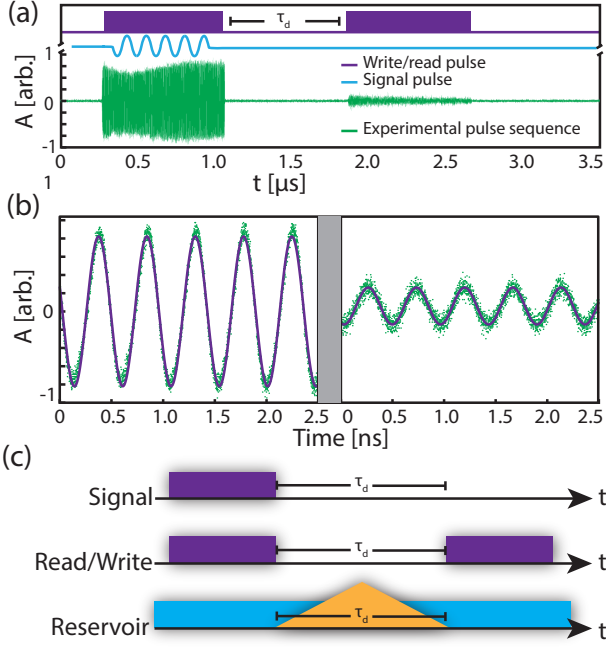


FIG. 6: (a) Timing diagram for optomechanical pulse storage, along with an example of a typical measure signal (purple). (b) Detail of a short section of the write (left panel) and read pulse (right panel). (c) Timing diagram for the storage enhancement and phase manipulation experiments described in the main text.

speed photodetector (New Focus 1554-B) whose output is high-pass filtered and electronically amplified before being sent to the VNA for measuring OMIT or a digital serial analyzer (DSA: Tektronix DSA70804B) for the pulse storage measurements.

In the pulse storage enhancement measurement an amplitude modulator ($A(t)$: EOSpace AZ-0K5-10-PFA-SFA) was added to the mode a laser to generate the optical pulses, while the phase modulator was used to generate the signal to be written. The signal to be written was a sine wave at ω_b generated by an arbitrary waveform generator (AWG: Tektronix AWG70002A) which was superimposed on the optical pulses generated by a low pass filtered pulse generator (PG: Stanford Research Systems DG535), triggered by the AWG. Here the reservoir mode control laser was operated in c.w. mode, however, during the phase manipulation measurement an amplitude modulator ($A(t)$: Lucent Technologies 2623CS) is added to the output of the laser, which was driven by a separate function generator to generate the phase manipulation pulses, as shown in Fig. 6. A thermoelectric heater/cooler was also placed under the sample and controlled with a PID for thermal stability during the measurement.

C. Mode characterization

The power spectral density for the radial breathing mode was measured using a high speed photodetector

and real time spectrum analyzer (Tektronix RSA5106A), and is shown in Fig. 7(b), which was carried out at low input power ($P_{\text{in}} \sim 50 \mu\text{W}$) to avoid optomechanical backaction. By fitting the power spectral density to a Lorentzian we extract a mechanical quality factor, $Q_m \sim 1.1 \times 10^4$, at room temperature and pressure. Optical transmission scans are shown in Fig. 7(c,d), with intrinsic quality factors labelled for each of the doublet modes. The per-photon optomechanical coupling rates were measured in a separate experiment, yielding g_r/α_r , $g_a/\alpha_a \sim 2\pi \times 25 \text{ kHz}$, where α_r and α_a are the strong control laser amplitudes for mode r , and a , respectively (see Supplementary Material).

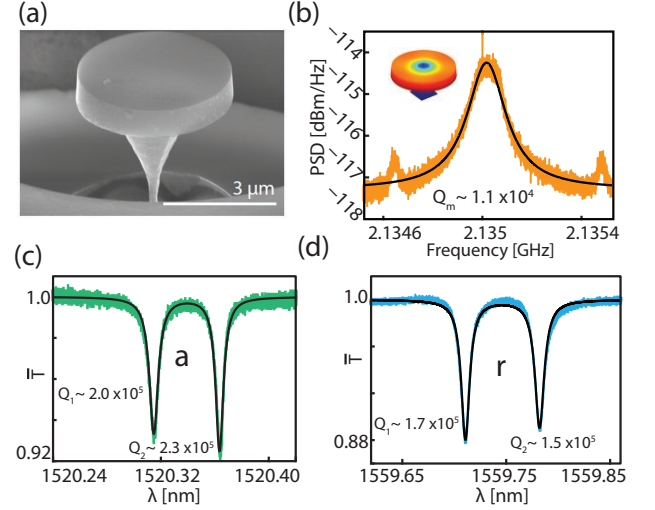


FIG. 7: (a) Scanning electron micrograph of the diamond microdisk used in this work. (b) Measured power spectral density of radial breathing mode at room temperature and pressure (inset: COMSOL simulated displacement profile). (c,d) Fiber taper transmission scans for both optical modes used in this work, revealing the doublet nature of the modes. Intrinsic optical quality factors are labelled.

In the limit that surface scattering effects are smaller than all other optical loss mechanisms ($g_{\text{ss}} \ll \kappa$), microdisks will possess degenerate clockwise and anticlockwise propagating modes, with negligible coupling between them. However, when the surface scattering approaches or exceeds the optical linewidth ($g_{\text{ss}} \geq \kappa$), the clockwise and counter clockwise modes couple and will form pairs of modes known as optical doublets. These are simply symmetric and antisymmetric combinations of the travelling wave modes. The orthogonality of the doublet modes allow us to calculate the overall mechanical frequency shift, or damping rate induced by a strong control laser by taking the sum of the contributions from the symmetric and antisymmetric mode.

AUTHOR CONTRIBUTIONS

D.P.L. and M.M. fabricated the device, performed the experiments, and analyzed the data. D.P.L. developed the theory. P.E.B. supervised the project. All authors contributed to writing the manuscript.

ACKNOWLEDGMENTS

The authors would like to thank Daniel Oblak and the QCloudLab for their generosity in lending us some of the components required to obtain these results. This work was supported by the National Research Council, Canadian Foundation for Innovation, Alberta Innovates, and the Natural Sciences and Engineering Research Council of Canada.

COMPETING INTERESTS

The authors declare no competing interests.

SUPPLEMENTARY INFORMATION

I. RESERVOIR ENGINEERING

The results of this work are enabled by dynamic manipulation of a mechanical oscillator through engineering the degrees of freedom it is coupled to. The manifestation of this coupling is optomechanical damping, and the optomechanical spring shift, which have been extensively studied in the past^{S1,S2}. These previous approaches leveraged frequency domain calculations and a Kubo formula to calculate damping rates, and the minimum phonon occupation. The frequency shift was then calculated through the Kramers Kronig relations. In our approach, we directly solve expressions in the time domain in the form of retarded Green's functions, and then adiabatically eliminate the fast dynamics of the cavity.

In the absence of optomechanical coupling, the mechanical mode is modelled as a damped harmonic oscillator, with annihilation operator \hat{b} , intrinsic frequency ω_b , and intrinsic damping rate Γ_b . The damping is a consequence of coupling to the environment, and according to the fluctuation-dissipation theorem this damping will be accompanied by a dissipation term. In the input-output formalism, we write

$$\dot{\hat{b}} = -\left(i\omega_b + \frac{\Gamma_b}{2}\right)\hat{b} + \sqrt{\Gamma_b}\hat{e}_{\text{in}}, \quad (\text{S1})$$

where \hat{e}_{in} is the input from the environment. ω_b and Γ_b are intrinsic properties of the device, however cavity optomechanics offers a way to manipulate the mechanical parameters of the cavity by optical means^{S3}. As we will show here, this can be viewed as coupling the mechanical mode to an optical reservoir mode, \hat{r} . Not only is this interaction easily controllable, but the reservoir can be arranged to have negligible thermal occupation through use of optical laser light.

We consider a reservoir mode with frequency ω_r connected to an input port at a rate κ_r^{ex} with a total decay rate κ_r . This is dissipatively coupled to the mechanical mode with a strength g_r . In the presence of a strong control laser with amplitude α_r , the optomechanical interaction can be linearized, and we can write expressions for the cavity fluctuation operator \hat{r} , which is coupled the mechanics at a rate $g_r = G_r\alpha_rx_o$, where $G_r = \frac{d\omega}{dx}$ is the shift in cavity frequency due mechanical displacement, and x_o are the zero point fluctuations of the mechanics^{S3}. This leads to the coupled equations of motion

$$\begin{bmatrix} \left(\frac{d}{dt} + \frac{1}{\chi_b}\right) & 0 & ig_r & ig_r \\ 0 & \left(\frac{d}{dt} + \frac{1}{\chi_{b^\dagger}}\right) & -ig_r & -ig_r \\ ig_r & ig_r & \left(\frac{d}{dt} + \frac{1}{\chi_r}\right) & 0 \\ -ig_r & -ig_r & 0 & \left(\frac{d}{dt} + \frac{1}{\chi_{r^\dagger}}\right) \end{bmatrix} \begin{bmatrix} \hat{b} \\ \hat{b}^\dagger \\ \hat{r} \\ \hat{r}^\dagger \end{bmatrix} = \begin{bmatrix} \sqrt{\Gamma_b}\hat{e}_{\text{in}} \\ \sqrt{\Gamma_b}\hat{e}_{\text{in}}^\dagger \\ \sqrt{\kappa_r^{\text{ex}}}\hat{r}_{\text{in}} \\ \sqrt{\kappa_r^{\text{ex}}}\hat{r}_{\text{in}}^\dagger \end{bmatrix}, \quad (\text{S2})$$

where we define the relevant response functions as $\chi_b^{-1}(\omega) = \Gamma_b/2 - i(\omega - \omega_b)$, $\chi_{b^\dagger}^{-1}(\omega) = \Gamma_b/2 - i(\omega + \omega_b)$, $\chi_r^{-1}(\omega) = \kappa_r/2 - i(\omega + \Delta_r)$, and $\chi_{r^\dagger}^{-1}(\omega) = \kappa_r/2 - i(\omega - \Delta_r)$. The input modes at time t , are given in terms of the time t_0 in the far past as^{S4}

$$\hat{e}_{\text{in}}(t) = \frac{1}{\sqrt{2\pi}} \int e^{-i\omega(t-t_0)} E_0(\omega) d\omega, \quad (\text{S3})$$

$$\hat{r}_{\text{in}}(t) = \frac{1}{\sqrt{2\pi}} \int e^{-i\omega(t-t_0)} R_0(\omega) d\omega, \quad (\text{S4})$$

where E_0 and R_0 are the state of the input modes at time t_0 . For the sake of simplicity, in what follows, we will assume $\kappa_r = \kappa_r^{\text{ex}}$.

Using Eq. S2, we can solve for the reservoir dynamics as

$$\hat{r}(t) = \hat{r}_0 e^{-(t-t_0)/\chi_r} + \int_{t_0}^t e^{-(t-t')/\chi_r} \left(\sqrt{\kappa_r} \hat{r}_{\text{in}} + iG_r \hat{b} + iG_r \hat{b}^\dagger \right) dt', \quad (\text{S5})$$

$$\hat{r}^\dagger(t) = \hat{r}_0^\dagger e^{-(t-t_0)/\chi_{r^\dagger}} + \int_{t_0}^t e^{-(t-t')/\chi_{r^\dagger}} \left(\sqrt{\kappa_r} \hat{r}_{\text{in}}^\dagger - iG_r \hat{b} - iG_r \hat{b}^\dagger \right) dt'. \quad (\text{S6})$$

It is interesting to note the role of the optical cavity as a filter. The exponential terms are in the form of a retarded Green's function, and specify a sensitivity to frequencies near $\pm\Delta_r$ to a history on the timescale $1/\kappa_r$.

Inserting this into the expression for the mechanics given in Eq. S2, we find an equation of motion for the mechanics under the influence of both the environment and the reservoir

$$\begin{aligned} \left(\frac{d}{dt} + i\omega_b \right) \hat{b} = & -\frac{\Gamma_b}{2} \hat{b} - |g_b|^2 \int_{t_0}^t \left(e^{-(t-t')/\chi_r} \hat{b}(t') - e^{-(t-t')/\chi_{r^\dagger}} \hat{b}(t') \right) dt' \\ & + \sqrt{\Gamma_b} \hat{e}_{\text{in}} + iG_b \sqrt{\kappa_r} \int_{t_0}^t \left(e^{-(t-t')/\chi_r} \hat{r}_{\text{in}}(t') + e^{-(t-t')/\chi_{r^\dagger}} \hat{r}_{\text{in}}^\dagger(t') \right) dt', \end{aligned} \quad (\text{S7})$$

where in the above we used the fact the $t - t_0 \gg 1/\kappa_r$ and applied the rotating wave approximation. The right side of the equation can be interpreted as the sum of damping and dissipation terms due to coupling to the environment, and damping and dissipation terms due to coupling to the reservoir. With the assumption that $\kappa_r \gg \Gamma_b$, we can make further simplifications. First we note that the integral associated with the dissipation term becomes

$$\begin{aligned} \int_{t_0}^t \left(e^{-(t-t')/\chi_r} + e^{-(t-t')/\chi_{r^\dagger}} \right) \hat{b}(t') dt' & \approx \int_{t_0}^t \left(e^{-(t-t')/\chi_r} - e^{-(t-t')/\chi_{r^\dagger}} \right) e^{i\omega_b(t-t')} \hat{b}(t') dt' \\ & = (\chi_r(\omega_b) - \chi_{r^\dagger}(\omega_b)) \hat{b}(t). \end{aligned} \quad (\text{S8})$$

Next we simplify the fluctuation term as

$$\begin{aligned} & \int_{t_0}^t \left(e^{-(t-t')/\chi_r} \hat{r}_{\text{in}}(t') + e^{-(t-t')/\chi_{r^\dagger}} \hat{r}_{\text{in}}^\dagger(t') \right) dt' \\ & = \frac{1}{\sqrt{2\pi}} \int \int_{t_0}^t \left(e^{(\chi_r^{-1} - i\omega)t'} e^{-\chi_r^{-1}t + i\omega t_0} \hat{R}_0(\omega) + e^{(\chi_{r^\dagger}^{-1} + i\omega)t'} e^{-\chi_{r^\dagger}^{-1}t - i\omega t_0} \hat{R}_0^\dagger(\omega) \right) dt' d\omega \\ & = \frac{1}{\sqrt{2\pi}} \int \left(\frac{e^{(\chi_r^{-1} - i\omega)t} - e^{(\chi_r^{-1} - i\omega)t_0}}{\chi_r^{-1} - i\omega} e^{-\chi_r^{-1}t + i\omega t_0} \hat{B}_0(\omega) + \frac{e^{(\chi_{r^\dagger}^{-1} + i\omega)t} - e^{(\chi_{r^\dagger}^{-1} + i\omega)t_0}}{\chi_{r^\dagger}^{-1} + i\omega} e^{-\chi_{r^\dagger}^{-1}t - i\omega t_0} \hat{R}_0^\dagger(\omega) \right) d\omega \\ & \approx \frac{1}{\sqrt{2\pi}} \int \left(e^{-i\omega(t-t_0)} \chi_r(\omega) \hat{R}_0(\omega) + e^{i\omega(t-t_0)} \chi_{r^\dagger}(\omega) \hat{R}_0^\dagger(\omega) \right) d\omega \\ & \approx \frac{1}{\sqrt{2\pi}} \int \left(e^{-i\omega(t-t_0)} \chi_b(\omega_b) \hat{R}_0(\omega) + e^{i\omega(t-t_0)} \chi_{r^\dagger}(\omega_b) \hat{R}_0^\dagger(\omega) \right) d\omega \\ & = \chi_r(\omega_b) \hat{r}_{\text{in}} + \chi_{r^\dagger}(\omega_b) \hat{r}_{\text{in}}^\dagger. \end{aligned} \quad (\text{S9})$$

where once again we used the assumption that $\kappa_r \gg \Gamma_b$ to simplify. Combining Eqs. S7–S9 we arrive at the solution

$$\begin{aligned} \left(\frac{d}{dt} + i\omega_b \right) \hat{b} = & - \left(\frac{\Gamma_b}{2} + |g_r|^2 \chi_r(\omega_b) - |g_r|^2 \chi_{r^\dagger}(\omega_b) \right) \hat{b} \\ & + \sqrt{\Gamma_b} \hat{e}_{\text{in}} + iG_r \sqrt{\kappa_r} \chi_r(\omega_b) \hat{r}_{\text{in}} + iG_r \sqrt{\kappa_r} \chi_{r^\dagger}(\omega_b) \hat{r}_{\text{in}}^\dagger. \end{aligned} \quad (\text{S10})$$

This can be rearranged to the simple expression reminiscent of Eq. S1

$$\dot{\hat{b}} = - \left(i\omega_b^{\text{eff}} + \frac{\Gamma_b^{\text{eff}}}{2} \right) \hat{b} + \sqrt{\Gamma_b} \hat{e}_{\text{in}} + g_r \sqrt{\kappa_r} \chi_r(\omega_b) \hat{r}_{\text{in}} + g_r \sqrt{\kappa_r} \chi_{r^\dagger}(\omega_b) \hat{r}_{\text{in}}^\dagger. \quad (\text{S11})$$

In the above we have absorbed a factor of i into the definition of R_0 and R_0^\dagger , and defined effective frequency and damping terms

$$\omega_b^{\text{eff}} = \omega_b + \omega_r^{\text{opt}} = \omega_b + |g_r|^2 \left(\frac{\omega_b + \Delta}{\kappa_r^2/4 + (\omega_b + \Delta_r)^2} + \frac{\omega_b - \Delta}{\kappa_r^2/4 + (\omega_b - \Delta_r)^2} \right), \quad (\text{S12})$$

$$\Gamma_b^{\text{eff}} = \Gamma_b + \Gamma_r^{\text{opt}} = \Gamma_b + |g_r|^2 \left(\frac{\kappa_r}{\kappa_r^2/4 + (\omega_b + \Delta_r)^2} - \frac{\kappa_r}{\kappa_r^2/4 + (\omega_b - \Delta_r)^2} \right). \quad (\text{S13})$$

Comparing Eq. S1 and Eq. S11, we see that coupling the reservoir mode induces both fluctuation and dissipation. By varying the strength or detuning of the control laser, the coupling to the reservoir is modified. In the sideband

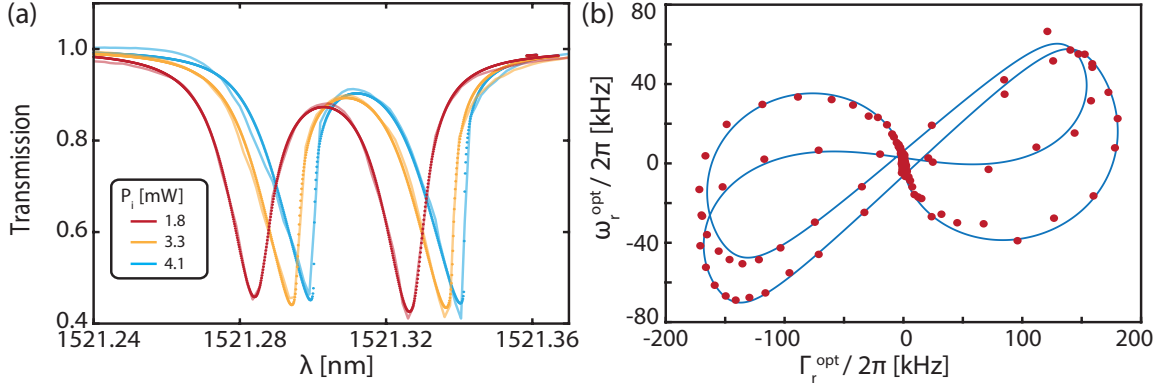


FIG. S1: (a) Optical transmission as a function of laser wavelength for the reservoir mode for increasing input power illustrating the relatively small thermo-optic shift. The $P_i = 1.8$ mW curve corresponds to the data presented in the main text. (b) Optomechanical damping and spring effect due to mode r plotted as functions of each other, corresponding to the data shown in the main text. Here the separation of each trajectory is due to a difference in the resonance contrast of each doublet mode.

resolved regime ($\omega_b \gg \kappa$) we note two special cases. For $\Delta_r = -\omega_b$ the effective interaction Hamiltonian is $H_{\text{eff}} = -g_r (\hat{b}^\dagger \hat{r} + \hat{b} \hat{r}^\dagger)$, and the mechanics has the equation of motion

$$\dot{\hat{b}} = -\left(i\omega_b + \frac{\Gamma_b}{2} + \frac{\Gamma_r^{\text{opt}}}{2}\right)\hat{b} + \sqrt{\Gamma_b}\hat{e}_{\text{in}} + \sqrt{\Gamma_r^{\text{opt}}}\hat{r}_{\text{in}}^\dagger. \quad (\text{S14})$$

On the other hand, for $\Delta_r = \omega_b$ the interaction Hamiltonian takes the form $H_{\text{eff}} = -g_r (\hat{b}\hat{r} + \hat{b}^\dagger\hat{r}^\dagger)$, and the equation of motion is

$$\dot{\hat{b}} = -\left(i\omega_b + \frac{\Gamma_b}{2} - \frac{\Gamma_r^{\text{opt}}}{2}\right)\hat{b} + \sqrt{\Gamma_b}\hat{e}_{\text{in}} + \sqrt{\Gamma_b}\hat{r}_{\text{in}}. \quad (\text{S15})$$

II. ENHANCED OMIT

The amplitude in cavity a , as a function of probe-control field detuning, δ_a , under the influence of the reservoir mode may be expressed as,

$$a(\delta_a) = -\frac{\sqrt{\kappa_{\text{ex}}}\hat{a}_{\text{in}}(\omega)}{i(-\omega_b + \delta_a) - \kappa_a/2 - \frac{|g_a|^2}{i(\omega_b + \omega_c^{\text{opt}} - \delta_a) + (\Gamma_b + \Gamma_r^{\text{opt}})/2}}. \quad (\text{S16})$$

When our probe is on-resonance, such that $\delta_a = \omega_b$, we can write our effective cooperativity as:

$$C_a^{\text{eff}} = C_a \frac{\Gamma_b}{\Gamma_{\text{eff}}}, \quad (\text{S17})$$

where $C_a = 4|g_a|^2/\Gamma_b\kappa_a$ is our baseline cooperativity.

A. Group delay

The group delay imparted on the pulse in transmission and reflection can be calculated about a central signal frequency, ω_s with the spectrum confined to a small window ($< \Gamma_b^{\text{eff}}$) following Safavi-Naeini et al.^{S5} by computing

$$\tau^{(T)} = \mathcal{R} \left\{ \frac{-i}{t(\omega_s)} \frac{dt}{d\omega} \right\}, \quad (\text{S18})$$

and

$$\tau^{(R)} = \mathcal{R} \left\{ \frac{-i}{r(\omega_s)} \frac{dt}{d\omega} \right\}, \quad (\text{S19})$$

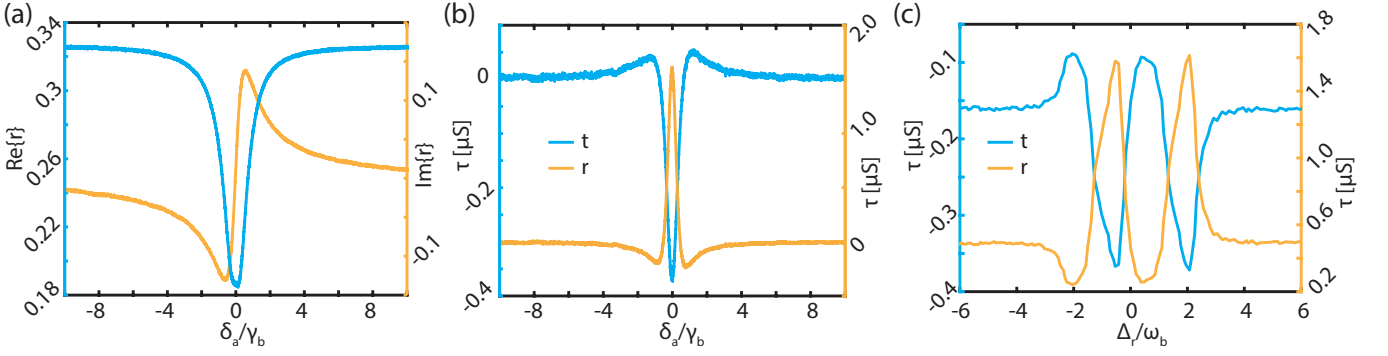


FIG. S2: (a) Real and imaginary parts of the OMIT scan corresponding to the maximum $C_{\text{eff}} = 83$, where δ_a is the probe field detuning. (b) Extracted group delay as a function δ_a , for fixed control laser detuning, $\Delta_a = \omega_b$. (c) Extracted group delay as a function of the reservoir mode detuning, Δ_r , for fixed probe laser detuning, $\delta_a = \omega_b$.

for the transmission and reflection group delay, respectively. These quantities are shown in Fig. S2 for both fixed and variable reservoir laser detuning.

III. COOLING AND HEATING

As a test of the reservoir engineering expressions, and as a step towards calculating the thermal occupations required for the memory calculations, we calculate full expressions for optomechanical heating and cooling here. Ignoring initial transients, the formal solution of Eq. S11 is

$$\hat{b}(t) = \int_{t_0}^t e^{-\left(i\omega_b^{\text{eff}} + \frac{\Gamma_b^{\text{eff}}}{2}\right)(t-\tau)} \left(\sqrt{\Gamma_b} \hat{e}_{\text{in}} + g_r \sqrt{\kappa_r} \chi_r(\omega_b) \hat{r}_{\text{in}} + g_r \sqrt{\kappa_r} \chi_r^\dagger(\omega_b) \right) d\tau. \quad (\text{S20})$$

We quantify the thermal statistics of the reservoir and environment with the correlators

$$\langle \hat{r}_{\text{in}}^\dagger(t) \hat{r}_{\text{in}}(t') \rangle = n_r^{\text{th}} \delta(t - t'), \quad (\text{S21})$$

$$\langle \hat{r}_{\text{in}}(t) \hat{r}_{\text{in}}^\dagger(t') \rangle = (n_r^{\text{th}} + 1) \delta(t - t'), \quad (\text{S22})$$

$$\langle \hat{e}_{\text{in}}^\dagger(t) \hat{e}_{\text{in}}(t') \rangle = n_e^{\text{th}} \delta(t - t'), \quad (\text{S23})$$

$$\langle \hat{e}_{\text{in}}(t) \hat{e}_{\text{in}}^\dagger(t') \rangle = (n_e^{\text{th}} + 1) \delta(t - t') \quad (\text{S24})$$

where n_r^{th} is the number of thermal photons occupying the reservoir, and n_e^{th} is the number of thermal phonons occupying the environment. Using these expressions, we can calculate the thermal occupancy of the cavity as

$$\begin{aligned} \langle \hat{b}^\dagger(t) \hat{b}(t) \rangle &= \int_{t_0}^t \int_{t_0}^t e^{-\left(-i\omega_b^{\text{eff}} + \frac{\Gamma_b^{\text{eff}}}{2}\right)(t-\tau) - \left(i\omega_b^{\text{eff}} + \frac{\Gamma_b^{\text{eff}}}{2}\right)(t-\tau')} \\ &\quad \left(\sqrt{\Gamma_b} \hat{e}_{\text{in}}(\tau) + g_r \sqrt{\kappa_r} \chi_r(\omega_b) \hat{r}_{\text{in}}(\tau) + g_r \sqrt{\kappa_r} \chi_r^\dagger \hat{r}_{\text{in}}^\dagger(\tau) \right) \times \\ &\quad \left(\sqrt{\Gamma_b} \hat{e}_{\text{in}}(\tau') + g_r \sqrt{\kappa_r} \chi_r(\omega_b) \hat{r}_{\text{in}}(\tau') + g_r \sqrt{\kappa_r} \chi_r^\dagger \hat{r}_{\text{in}}^\dagger(\tau') \right) d\tau d\tau' \\ &= \int_{t_0}^t e^{\Gamma_b^{\text{eff}}(t-\tau)} \left(\Gamma_b n_{\text{th},b} + \kappa_r |g_r \chi_r(\omega_b)|^2 n_{\text{th},b} + \kappa_r |g_r \chi_r^\dagger(\omega_b)|^2 (n_{\text{th},b} + 1) \right) d\tau \\ &= \frac{\Gamma_b n_{\text{th},b} + \kappa_r |g_r \chi_r(\omega_b)|^2 n_{\text{th},b} + \kappa_r |g_r \chi_r^\dagger(\omega_b)|^2 (n_{\text{th},b} + 1)}{\Gamma_b^{\text{eff}}} \end{aligned} \quad (\text{S25})$$

$$(\text{S26})$$

In the experiment considered in this work, our reservoir does not have thermal occupation. Setting $n_r^{\text{th}} = 0$ we recover the usual limit of optomechanical cooling

$$\langle \hat{n} \rangle = \frac{\Gamma_b n_e^{\text{th}} + \Gamma_{\text{opt}}^r n^{\text{min}}}{\Gamma_b + \Gamma_{\text{opt}}^r} \quad (\text{S27})$$

where, $n^{\text{min}} = |g_r|^2 \kappa_r \chi_r^\dagger(\omega_b) / \Gamma_r^{\text{opt}}$.

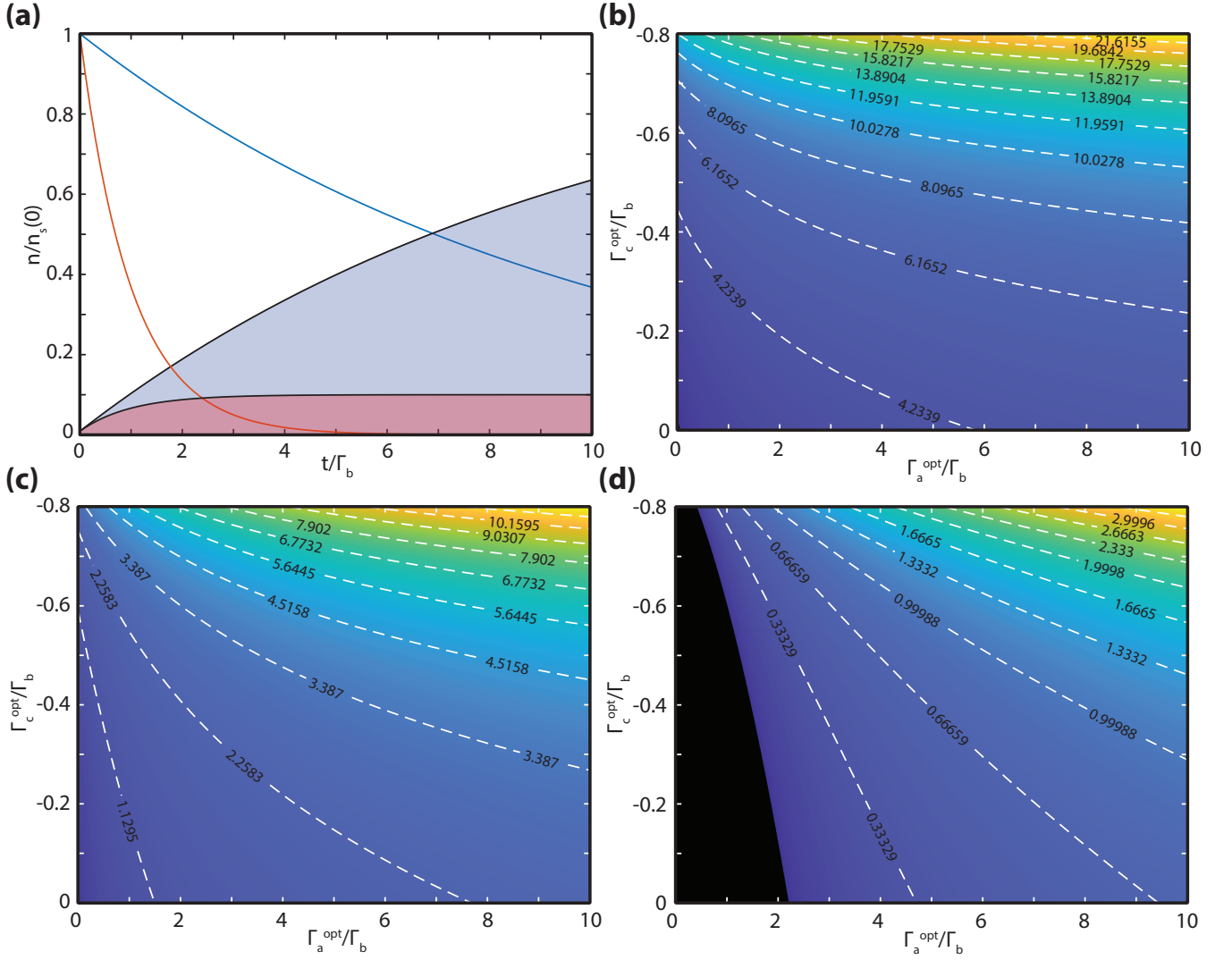


FIG. S3: (a) Signal phonons (solid lines) and thermal phonons (shaded curves) plotted for $\Gamma_c^{\text{opt}}/\Gamma_b = 0$ (red) and $\Gamma_c^{\text{opt}}/\Gamma_b = -0.9$ (blue). The initial signal to noise ratio $n_s(0)/n_{\text{th}}(0) = 10$, and $\Gamma_a^{\text{opt}}/\Gamma_b = 10$. (b-d) $t_s \Gamma_b$ vs. optomechanical damping rates for initial signal to noise ratios $n_s(0)/n_{\text{th}}(0) = \{10, 1, 0.1\}$.

IV. STORAGE ENHANCEMENT

Solving the equations of motion explicitly, we can divide the phonon population in the cavity during the storage time into signal phonons, which are proportional to \hat{a}_{in} , and undesired thermal phonons, which are a consequence of \hat{e}_{in} . These each evolve as,

$$\langle \hat{b}_s^\dagger(t) \hat{b}_s(t) \rangle = \langle \hat{b}_s^\dagger(0) \hat{b}_s(0) \rangle e^{-\Gamma_b^{\text{eff}} t} \quad (\text{S28})$$

$$\langle \hat{b}_{\text{th}}^\dagger(t) \hat{b}_{\text{th}}(t) \rangle = n_e^{\text{th}} \Gamma_b \left(\frac{e^{-\Gamma_b^{\text{eff}} t}}{\Gamma_b + \Gamma_a^{\text{opt}}} + \frac{1 - e^{-\Gamma_b^{\text{eff}} t}}{\Gamma_b + \Gamma_c^{\text{opt}}} \right). \quad (\text{S29})$$

Defining the storage time as the moment the signal level decays to the level of the thermal phonons, we find,

$$t_s = \frac{1}{\Gamma_b + \Gamma_c^{\text{opt}}} \ln \left(\frac{n_s(0)}{n_{\text{th}}(0)} + \frac{\Gamma_a^{\text{opt}} - \Gamma_c^{\text{opt}}}{\Gamma_b + \Gamma_a^{\text{opt}}} \right). \quad (\text{S30})$$

V. PHASE SHIFTING

Reservoir engineering also allows us to dynamically change the frequency of the mechanical mode. If the frequency is changed over a time interval δt , the change in phase may be expressed as,

$$\delta\phi = \int_0^{\delta t} (\omega_b(t) - \omega_b(0)) dt \quad (\text{S31})$$

For simplicity, we assume we change our mechanical frequency as a ramp function, with maximum frequency shift $\delta\omega_b$. Under the adiabaticity requirement $1 \gg \frac{\delta\omega_b}{\omega_b}$. This yields the simple expression for the phase shift,

$$\delta\phi = \frac{\delta\omega_b \delta t}{2}. \quad (\text{S32})$$

In the phase shifting experiment in the main text, we operate with the reservoir laser detuning $\Delta_r \approx -\omega_b$, so we may approximate the frequency shift as,

$$\delta\omega_b \approx \frac{|g_r|^2(\Delta_r - \omega_b)}{(\Delta_r - \omega_b)^2 + \kappa_r^2/4}. \quad (\text{S33})$$

VI. PULSE COMPRESSION

The reservoir mode also permits the mechanical damping rate to be dynamically adjusted. For example, at $\Delta_r \approx -\omega_b$, the damping is approximately,

$$\Gamma_r^{\text{opt}} \approx \frac{-\kappa_r |g_r|^2/2}{(\Delta_r - \omega_b)^2 + \kappa_r^2/4}. \quad (\text{S34})$$

If we ramp the mechanical damping according the expression $\Gamma_r^{\text{opt}}(t) = \eta t$, we recover the expression for a time lens^{S6},

$$\langle \hat{b}_s^\dagger(t) \hat{b}_s(t) \rangle = \langle \hat{b}_s^\dagger(0) \hat{b}_s(0) \rangle e^{-(\Gamma_b t + \eta t^2)}. \quad (\text{S35})$$

[S1]F. Marquardt, J. P. Chen, A. A. Clerk, and S. M. Girvin, Phys. Rev. Lett. **99**, 093902 (2007).

[S2]I. Wilson-Rae, N. Nooshi, W. Zwerger, and T. J. Kippenberg, Phys. Rev. Lett. **99**, 093901 (2007).

[S3]M. Aspelmeyer, T. J. Kippenberg, and F. Marquardt, Rev. Mod. Phys. **86**, 1391 (2014).

[S4]C. W. Gardiner and P. Zoller, *Quantum Noise* (Springer, Berlin, 1991) Chap. 4, pp. 106–111.

[S5]A. H. Safavi-Naeini, T. M. Alegre, J. Chan, M. Eichenfield, M. Winger, Q. Lin, J. T. Hill, D. Chang, and O. Painter, Nature **472**, 69 (2011).

[S6]G. Patera, J. Shi, D. B. Horoshko, and M. I. Kolobov, J. Opt. **19**, 054001 (2017).